Monoligated Monovalent Ni: the $3d_{Ni}^9$ Manifold of States of NiCu and Comparison to the $3d^9$ States of AlNi, NiH, NiCl, and NiF†

Gretchen K. Rothschopf and Michael D. Morse*
Department of Chemistry, University of Utah, Salt Lake City, Utah 84112
Received: June 7, 2005; In Final Form: August 11, 2005

A dispersed fluorescence investigation of the low-lying electronic states of NiCu has allowed the observation of four out of the five states that derive from the $3d_{Ni}^9\ 3d_{Cu}^{10}\ \sigma^2$ manifold. Vibrational levels of the ground $X^2\Delta_{5/2}$ state corresponding to $v = 0-11$ are observed and are fit to provide $\omega_e = 275.93 \pm 1.06$ cm^{-1} and $\omega_e x_e = 1.44 \pm 0.11$ cm^{-1}. The $v = 0$ levels of the higher lying states deriving from the $3d_{Ni}^9\ 3d_{Cu}^{10}\ \sigma^2$ manifold are located at 912, 1466, and 1734 cm^{-1}, and these states are assigned to Ω values of $^3/_2$, $^1/_2$, and $^3/_2$, respectively. The last of these assignments is based on selection rules and is unequivocal; the first two are based on a comparison to ab initio and ligand field calculations and could conceivably be in error. It is also possible that the $v = 0$ level of the state found at 912 cm^{-1} is not observed, so that T_0 for the lowest excited state actually lies near 658 cm^{-1}. These results are modeled using a matrix Hamiltonian based on the existence of a ground manifold of states deriving from the $3d^9$ configuration on nickel. This matrix Hamiltonian is also applied to the spectroscopically well-known molecules AlNi, NiH, NiCl, and NiF. The term energies of the $^2\Sigma^+$, $^2\Pi$, and $^2\Delta$ states of these molecules, which all derive from a $3d^9$ configuration on the nickel atom, display a clear and understandable trend as a function of the electronegativity of the ligands.

I. Introduction

A significant number of monoligated nickel molecules are now spectroscopically known in which the nickel atom is bound to a monovalent atomic or diatomic ligand. These molecules include NiH,[1−9] NiCu,[10,11] NiAu,[12,13] AlNi,[13,14] NiF,[15−20] NiCl,[21−26] NiBr,[27,28] NiI,[29,30] and NiCN.[31,32] In all of these molecules, chemical bonding occurs when the Ni atom in its $3d^94s^1$, ^3D state bonds to the ligand by spin-pairing the $4s^1$ electron of nickel with a σ^1 electron of the ligand. The σ electron can be an s electron (as in NiH, NiCu, or NiAu), a pσ electron (as in AlNi, NiF, and NiCl), or an electron in a σ orbital of the diatomic ligand, as in NiCN. In some cases, such as NiF and NiCl, it may be more appropriate to think of the low-lying electronic states as arising from a $3d^9$ Ni^+ cation interacting with a closed-shell F^- or Cl^- anion. In all cases, however, an open shell $3d^9$ core remains on the Ni atom. It is of interest to investigate how the 10-fold degeneracy of the $3d^9$ core is split in the presence of the ligand, so that we may understand the chemical bonding and electronic structure of these species in more detail. In this article, we report the results of a dispersed fluorescence investigation of NiCu and make comparisons of its electronic energy levels with those of the other molecules.

The first spectroscopic study of diatomic NiCu was performed by Fu et al., in 1989[10] and expanded by Spain et al., in 1992.[11] In both investigations, resonant two photon ionization (R2PI) methods were employed in conjunction with a laser ablation/supersonic expansion source to record the optical spectra of the NiCu molecule. This led to the identification of nine electronic band systems in the range of 10 400−16 500 cm^{-1}. The Ω values were determined for eight out of the nine excited states and for the ground state by analysis of rotationally resolved spectra. All of the excited states were assumed to derive from the $3d_{Ni}^8\ (^3F)3d_{Cu}^{10}\ \sigma^2\sigma^{*1}$ electronic manifold, a possibility that was supported by a ligand field analysis of this manifold[33] and by considerations of the possible separated atom limits. The ground state was assumed to derive from the $3d_{Ni}^9\ 3d_{Cu}^{10}\ \sigma^2$ manifold and was found to possess $\Omega = {}^5/_2$, a result which implied a $^2\Delta_{5/2}$ ground term. This in turn indicated that the 3d orbitals are substantially uninvolved in the chemical bonding. The emergence of $^2\Delta_{5/2}$ as the ground state of NiCu was predicted by ab initio quantum chemistry[34] and was also explained on the basis of a ligand field investigation of the $3d_{Ni}^9\ 3d_{Cu}^{10}\ \sigma^2$ manifold.[33]

The $3d_{Ni}^9\ 3d_{Cu}^{10}\ \sigma^2$ manifold of states leads to $^2\Sigma^+$, $^2\Pi$, and $^2\Delta$ states in Hund's case (a), but spin−orbit interaction splits and mixes these states to give a single $\Omega = {}^5/_2$ state, which is the $^2\Delta_{5/2}$ ground state, two $\Omega = {}^3/_2$ states, which are mixtures of the $^2\Delta_{3/2}$ and $^2\Pi_{3/2}$ states, and two $\Omega = {}^1/_2$ states, which are mixtures of the $^2\Pi_{1/2}$ and $^2\Sigma_{1/2}{}^+$ states. The aim of the present dispersed fluorescence study is to locate these low-lying states of NiCu and to compare their energies to the results of ab initio quantum chemistry[4] and the ligand field model.[33]

II. Experimental Section

The dispersed fluorescence instrument employed in this study consists of a laser ablation-supersonic expansion source,[35] a set of F/6.6 collection optics, and an F/6.5 spectrograph equipped with a gated, intensified, CCD array detector. The basic instrument has been previously described in detail.[36] The NiCu molecules were produced by focusing the fundamental radiation from a Nd:YAG laser (15−20 mJ/pulse) onto a resurfaced U.S. nickel coin that was rotated and translated using a mechanism similar to that described by O'Brien et al.[37] The 1:3 ratio of Ni:Cu in this alloy assisted in reducing the concentration of Ni_2 relative to NiCu, as compared to an equimolar alloy, thereby reducing the intensity of any Ni_2 fluorescence that might be incidentally excited while tuning the excitation radiation to an absorption of NiCu. This was desirable given the high density of vibronic states previously observed in the spectrum of Ni_2.[38,39] The metal-containing plasma formed by the laser ablation process was then entrained in a pulse of helium carrier gas,

† Part of the special issue "Jack Simons Festschrift".
* Corresponding author. E-mail: morse@chemistry.chem.utah.edu.

10.1021/jp053022m CCC: $30.25
Published on Web 09/22/2005

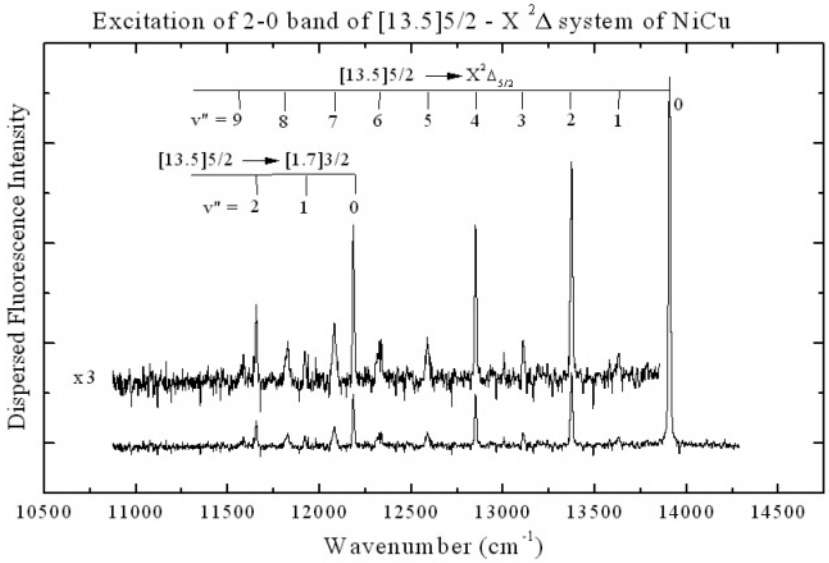

Figure 1. Dispersed fluorescence spectrum of NiCu resulting from excitation of the 2−0 band of the $[13.5]^5/_2 \leftarrow X^2\Delta_{5/2}$ band system. Two vibrational progressions are observed and identified: a more intense progression to the $X^2\Delta_{5/2}$ ground state and a weaker progression to the low-lying $[1.7]^3/_2$ state.

which originated from a reservoir that was held at 110 psig behind a double solenoid pulsed valve.[35] Following laser ablation of the NiCu alloy, the molecular beam and its contents traveled through a channel 5.5 cm long and 1.5 mm in diameter before undergoing supersonic expansion into vacuum (2×10^{-4} Torr) from a final orifice 2.5 mm in diameter.

A dye laser (Lambda Physik, FL2002) pumped by the second (532 nm) or third (355 nm) harmonic radiation of a second Nd:YAG laser (Continuum, Surelite II-10) was used to excite the molecules about 1 cm downstream from the exit orifice. The excitation radiation crossed the molecular beam at right angles, and fluorescence was collected at right angles to both the molecular beam and the excitation radiation. Emission from the molecular beam was imaged onto the entrance slit of an 0.5 m spectrograph (Acton Research Corp., model SpectraPro-556) equipped with a gated, intensified, charge coupled device mounted at the exit focal plane (Roper Scientific, model RE/ICCD EEV 576 × 384 CCD and model PG-10 Pulse Generator). The instrument was calibrated using well-known emission lines of Ar, Ne, and Hg excited in hollow cathode discharge tubes (Photron, Ltd.; Perkin-Elmer), in conjunction with the accepted vacuum wavelengths tabulated in the MIT Wavelength Tables.[40] The data were collected and stored using software accompanying the ICCD and its peripherals (Roper Scientific, Winspec V.1.6.2). The timing of the pulsed nozzle, ablation laser pulse, excitation laser pulse, and detection trigger were controlled using a 386-based personal computer equipped with a timing control card that was custom-built in the Electronics Shop at the University of Utah.

III. Results

Figure 1 presents a dispersed fluorescence spectrum of NiCu resulting from excitation of the 2−0 band of the $[13.5]^5/_2 \leftarrow X^2\Delta_{5/2}$ band system. The nomenclature used here to identify the $[13.5]^5/_2$ upper state begins with the energy of the state in units of 10^3 cm^{-1} [in square brackets] and is followed by the Ω value of the state. Two vibrational progressions are observed in the dispersed fluorescence spectrum: a more intense progression in the ground state and a weaker progression in a low-lying excited state. The ground state progression extends out to $v'' = 9$, whereas the excited state progression only displays transitions to $v'' = 0$, 1, and 2. It is likely that fluorescence to higher vibrational levels of both states occurs, but the response of the photocathode of the intensified CCD detector is very poor for wavenumbers below 11 200 cm^{-1}, preventing detection of higher vibrational levels. Excitation of other vibronic levels of NiCu has allowed the $v'' = 10$, 11 levels to be observed for the ground $X^2\Delta_{5/2}$ state. The dispersed fluorescence signal for NiCu was extremely weak and thus the $v'' = 0$ peak of the ground state progression is mostly due to scattered excitation radiation. In part, the signal was weak because of the long lifetime of the $[13.5]^5/_2$ state (4.7 μs). The spectrum displayed in Figure 1 represents the summed signal obtained by dispersing the fluorescence from 15 000 experimental cycles (25 min).

Allowed emissions from the $[13.5]^5/_2$ excited state must terminate on levels with $\Omega'' = {}^7/_2$, $^5/_2$, or $^3/_2$. The $3d_{Ni}{}^9\ 3d_{Cu}{}^{10}\ \sigma^2$ manifold of states generates only one state corresponding to the $\Omega = {}^5/_2$ possibility, which is the $X^2\Delta_{5/2}$ ground state. This $3d_{Ni}{}^9\ 3d_{Cu}{}^{10}\ \sigma^2$ configuration also generates two $\Omega = {}^3/_2$ and two $\Omega = {}^1/_2$ states. Considering that the low-lying states observed must arise from the $3d_{Ni}{}^9\ 3d_{Cu}{}^{10}$ configuration and must be allowed under electric dipole selection rules, the second vibrational progression observed in Figure 1 must terminate on a low-lying electronic state with $\Omega'' = {}^3/_2$, which we designate as the $[1.7]^3/_2$ state. Vibrational progressions in the ground state and in the $[1.7]^3/_2$ state were observed following excitation of the 1−0, 2−0, 3−0, 4−0, and 5−0 bands of the $[13.5]^5/_2 \leftarrow X^2\Delta_{5/2}$ band system.

The dispersed fluorescence spectrum obtained by excitation of the 2−0 band of the $[13.1]^3/_2 \leftarrow X^2\Delta_{5/2}$ system of NiCu is displayed in Figure 2. Four vibrational progressions are observed, including a long progression to the ground state and a shorter progression to the $[1.7]^3/_2$ state that was observed in fluorescence from the $[13.5]^5/_2$ state. As in the previous example, the intense peak at the excitation frequency is mostly due to scattered excitation radiation. The remaining two progressions have the possibility of terminating on $\Omega'' = {}^5/_2$, $^3/_2$, or $^1/_2$ according to electric dipole selection rules. There are only three possibilities remaining from the $3d_{Ni}{}^9\ 3d_{Cu}{}^{10}\ \sigma^2$ electron configuration, however: one $\Omega = {}^3/_2$ and two $\Omega = {}^1/_2$ states. Ligand field calculations[33] and ab initio results[34] (in parentheses) predict $\Omega = {}^3/_2$ states at 798 (719) cm^{-1} and 2098 (1952) cm^{-1}. The $\Omega = {}^1/_2$ states are predicted at 1776 (1602) cm^{-1} and 3346 (3239) cm^{-1}. Based on these theoretical results, it is likely that

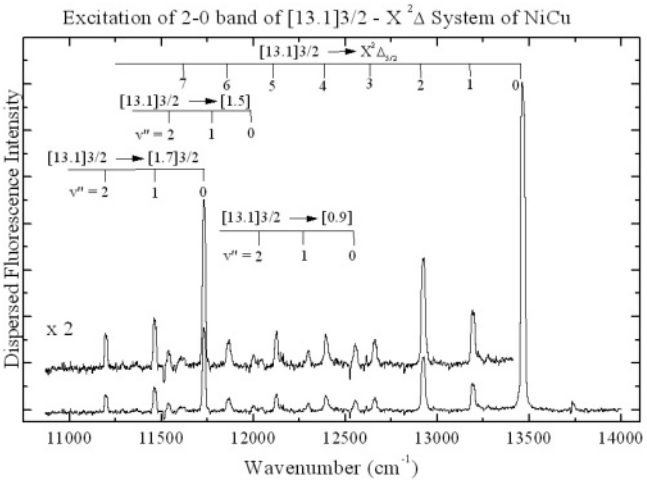

Figure 2. Dispersed fluorescence spectrum of NiCu obtained by excitation of the 2−0 band of the $[13.1]^3/_2 \leftarrow X^2\Delta_{5/2}$ system. Four vibrational progressions are observed, including a long progression to the ground state and a shorter progression to the $[1.7]^3/_2$ state that was observed in Figure 1. The remaining two progressions are to the $[0.9]^3/_2$ and $[1.5]^1/_2$ states, where the Ω assignments are based on a comparison to theory.

TABLE 1: Dispersed Fluorescence Excitation and Emission Bands of NiCu

excitation		emission observed to			
band system	$v'-v''$	$X^2\Delta_{5/2}$	$[0.9]^3/_2$[a]	$[1.5]^1/_2$[a]	$[1.7]^3/_2$
$[13.5]^5/_2 \leftarrow X^2\Delta_{5/2}$	0−0	0−4, 8			0−2
	1−0	0−7			0−2
	2−0	0−9			0−4
	3−0	0−10			0−4
	4−0	0−8, 10, 11			0, 1, 3, 4
$[13.1]^3/_2 \leftarrow X^2\Delta_{5/2}$	1−0	0−5	0, 2	0, 2	0, 1
	2−0	0−8	0−2	0, 2	0−2
	3−0	0−6	1	0, 2, 3	0, 1
	4−0	0−4, 6−8	0	0, 3	0−2
	5−0	0−4			1, 2

[a] For the [0.9] and [1.5] states the experimental data do not establish the value of Ω. However, the assignments as $[0.9]^3/_2$ and $[1.5]^1/_2$ are in reasonable agreement with both ab initio and ligand field theory.

the progression starting at 912 cm^{-1} relative to the excitation frequency represents fluorescence to the $\Omega = {}^3/_2$ state that is predicted at 798 (719) cm^{-1}. The other new progression, which begins at 1466 cm^{-1}, probably corresponds to fluorescence to the $\Omega = {}^1/_2$ state predicted at 1776 (1602) cm^{-1}. These two states are designated as $[0.9]^3/_2$ and $[1.5]^1/_2$, but it should be remembered that the assignment of the Ω quantum number is based entirely on the comparison to ab initio and ligand field calculations.

Excitation of the 4−0 and 6−0 bands of the $[11.9]^5/_2 \leftarrow X^2\Delta_{5/2}$ system was attempted to try to confirm the Ω value of the [0.9] state as $\Omega = {}^3/_2$. However, the fluorescence observed was very weak and it could not be conclusively determined that fluorescence to the [0.9] state was observed. Thus, the Ω values of the [0.9] and [1.5] states remain experimentally unknown, although the comparison to theory strongly suggests that these are the $[0.9]^3/_2$ and $[1.5]^1/_2$ states, respectively.

A list of the bands excited and the resulting fluorescence bands observed is provided in Table 1. The vibrational constants of the low-lying states were obtained by combining the data from all of the dispersed fluorescence experiments into a single global fit for each lower state. This was done by subtracting the wavenumbers of the fluorescence bands from the excitation wavenumber to provide the energies of the lower states relative to the $v = 0$ level of the ground state. When the same vibrational level was observed in more than one dispersed fluorescence experiment, its average wavenumber and standard deviation were calculated using standard formulas.[41] Fitted values of the vibrational constants T_0, ω_e'', and $\omega_e''x_e''$ were then obtained by a linear least-squares fit of the measured energy levels to the expression

$$E_v = T_0 + \omega_e''v - \omega_e''x_e''(v^2 + v) \quad (1)$$

The vibronic levels identified from this work are listed in Table 2 and calculated vibrational constants are provided in Table 3.

TABLE 2: Vibronic Energy Levels of NiCu

electronic state	v''	average relative wavenumber (cm^{-1})	fitted wavenumber (cm^{-1})	residual (cm^{-1})
$X^2\Delta_{5/2}$	0	0	0.45	−0.45
	1	276.87 ± 3.82	273.44	3.43
	2	544.17 ± 2.40	543.48	0.69
	3	809.12 ± 2.83	810.59	−1.47
	4	1072.32 ± 2.49	1074.76	−2.44
	5	1336.17 ± 3.18	1335.98	0.19
	6	1599.27 ± 3.07	1594.26	5.01
	7	1849.46 ± 2.12	1849.61	−0.15
	8	2100.52 ± 2.76	2102.01	−1.49
	9	2345.84 ± 9.16	2351.47	−5.63
	10	2605.56 ± 7.65	2597.99	7.57
	11	2837.79 ± 8.96	2841.57	−3.76
$[0.9]^3/_2$[a]	0	912.41 ± 3.46	912.41	
	1	1167.51 ± 5.03	1167.52	
	2	1423.52 ± 5.21	1423.52	
$[1.5]^1/_2$[a]	0	1465.91 ± 2.25	1465.91	
	2	1928.06 ± 4.65	1928.06	
	3	2128.47 ± 3.77	2128.47	
$[1.7]^3/_2$	0	1733.97 ± 2.28	1734.47	−0.49
	1	1999.93 ± 2.45	1998.85	1.08
	2	2262.20 ± 3.42	2262.47	−0.27
	3	2524.58 ± 3.92	2525.30	−0.72
	4	2787.78 ± 4.04	2787.37	0.41

[a] For the [0.9] and [1.5] states the experimental data do not establish the value of Ω. However, the assignments as $[0.9]^3/_2$ and $[1.5]^1/_2$ are in reasonable agreement with both ab initio and ligand field theory. For these states only three vibrational levels are observed, giving an exact fit for the values of T_0, ω_e, and $\omega_e x_e$. Accordingly, no error limits can be associated with these parameters.

TABLE 3: Fitted Vibrational Constants for NiCu

state	T_0 (cm^{-1})	ω_e (cm^{-1})	$\omega_e x_e$ (cm^{-1})
$[1.7]^3/_2$	1733.9 ± 0.98	265.16 ± 1.43	0.386 ± 0.28
$[1.5]^1/_2$[a]	1465.9[a]	261.74[a]	10.22[a]
$[0.9]^3/_2$[a]	912.4[a]	254.21[a]	0.45[a]
$X^2\Delta_{5/2}$	0	275.93 ± 1.06	1.44 ± 0.11

[a] For the $[1.5]^1/_2$ and $[0.9]^3/_2$ states only three vibrational levels were observed, making it possible to solve for T_0, ω_e, and $\omega_e x_e$ exactly. As a result it was not possible to estimate the errors in these parameters. In all other cases the quoted error limits represent the 1σ standard deviation of the fit. For the $[1.5]^1/_2$ and $[0.9]^3/_2$ states the experimental data do not establish the value of Ω. However, the assignments as $[1.5]^1/_2$ and $[0.9]^3/_2$ are in reasonable agreement with both ab initio and ligand field theory.

IV. Discussion

A. Application of Ligand Field Theory to NiCu. The four observed electronic states deriving from the $3d_{Ni}^9\ 3d_{Cu}^{10}\ \sigma^2$ manifold in NiCu fall somewhat close to the energies calculated by both ab initio[34] and ligand field methods,[33] as is displayed in Table 4. In this table the CASSCF calculation of Shim, which allowed full reorganization of the electrons within the 3d and 4s subshells, followed by configuration interaction and calculation of spin−orbit effects, is provided for comparison to experiment and to the ligand field calculations. The ligand field calculations reported here use the ligand-field Hamiltonian[33]

$$\underline{\underline{\mathbf{H}}} = \begin{array}{c} \begin{matrix} {}^2\Sigma^+_{1/2} & {}^2\Pi_{1/2} & {}^2\Pi_{3/2} & {}^2\Delta_{3/2} & {}^2\Delta_{5/2} \end{matrix} \\ \begin{pmatrix} \frac{2}{7}(B_0^{\,2} + B_0^{\,4}) & -\sqrt{\frac{3}{2}}\zeta & 0 & 0 & 0 \\ -\sqrt{\frac{3}{2}}\zeta & \frac{1}{7}B_0^{\,2} - \frac{4}{21}B_0^{\,4} + \frac{\zeta}{2} & 0 & 0 & 0 \\ 0 & 0 & \frac{1}{7}B_0^{\,2} - \frac{4}{21}B_0^{\,4} - \frac{\zeta}{2} & -\zeta & 0 \\ 0 & 0 & -\zeta & -\frac{2}{7}B_0^{\,2} + \frac{1}{21}B_0^{\,4} + \zeta & 0 \\ 0 & 0 & 0 & 0 & -\frac{2}{7}B_0^{\,2} + \frac{1}{21}B_0^{\,4} - \zeta \end{pmatrix} \end{array} \quad (2)$$

where $B_0^k = Z_L e^2 \langle r^k \rangle / R^{k+1}$, and Z_L is the effective charge of the Cu ligand, e is the charge of the electron, $\langle r^k \rangle$ is the radial expectation value of the nickel 3d orbital, as calculated by numerical Hartree−Fock[42] or Dirac−Fock[43] methods, R is the internuclear separation of the NiCu molecule, which has been measured to be $r_0 = 2.2346 \pm 0.0005$ Å,[11] and ζ is the spin−orbit parameter for a nickel 3d orbital.

The ligand field calculation designated as ligand field 1 in Table 4 was reported in our previous publication on the application of ligand field methods to NiCu.[33] That calculation employed a realistic value of the spin−orbit parameter of $\zeta = 603.0$ cm^{-1} but used radial expectation values taken from Dirac−Fock calculations on the $3d^84s^2$, ^{3}F state of atomic nickel.[43] This is inappropriate given that the states of the $3d_{Ni}^9\ 3d_{Cu}^{10}\ \sigma^2$ manifold of NiCu correlate to the Ni $3d^94s^1$, ^{3}D + Cu $3d^{10}4s^1$, ^{2}S separated atom limit.

The calculation designated as ligand field 2 in Table 4 attempts to correct for this error by scaling the radial expectation values obtained using a numerical Hartree−Fock calculation on the $3d^94s^1$, ^{3}D state of atomic nickel[42] by the published correction factors between the relativistic Dirac−Fock and the nonrelativistic Hartree−Fock calculations.[43] The radial expectation values change significantly when the electronic configuration is changed from $3d^84s^2$, ^{3}F to $3d^94s^1$, ^{3}D, and this affects the calculated energies considerably. Unfortunately, this modification worsens the agreement between the ligand field model and experiment.

To determine whether the low-lying states of NiCu could be described as simple mixtures of the $^2\Sigma_{1/2}{}^+$, $^2\Pi_{1/2,3/2}$, and $^2\Delta_{3/2,5/2}$ states that differ only in the location of the hole in the 3d orbitals of nickel, an attempt was made to fit the observed energy levels to a model in which the term energies of the $^2\Sigma^+$, $^2\Pi$, and $^2\Delta$ states in the absence of spin−orbit interaction are given by T_Σ, T_Π, and T_Δ, respectively. When the spin−orbit interaction is included, a matrix representation of the spin−orbit operator provides the Hamiltonian matrix:

$$\underline{\underline{\mathbf{H}}} = \begin{array}{c} \begin{matrix} {}^2\Sigma^+_{1/2} & {}^2\Pi_{1/2} & {}^2\Pi_{3/2} & {}^2\Delta_{3/2} & {}^2\Delta_{5/2} \end{matrix} \\ \begin{pmatrix} T_\Sigma & -\sqrt{\frac{3}{2}}\zeta & 0 & 0 & 0 \\ -\sqrt{\frac{3}{2}}\zeta & T_\Pi + \frac{\zeta}{2} & 0 & 0 & 0 \\ 0 & 0 & T_\Pi - \frac{\zeta}{2} & -\zeta & 0 \\ 0 & 0 & -\zeta & T_\Delta + \zeta & 0 \\ 0 & 0 & 0 & 0 & T_\Delta - \zeta \end{pmatrix} \end{array} \quad (3)$$

The quantities T_Σ, T_Π, and T_Δ were then varied to perform a least-squares fit of the measured energy levels, with ζ fixed at the value 603 cm^{-1}. Again, rather poor agreement with experiment was obtained, as is evident from the entry in Table 4 labeled Fit 3.

The model used in eq 3 provides complete flexibility for the energetics of the $^2\Sigma^+$, $^2\Pi$, and $^2\Delta$ states in the absence of spin−orbit interaction and then applies a correction for the spin−orbit interaction based on these states being well-described by a single configuration in which the hole is in a nickel 3d orbital. Surprisingly, this model fails to reproduce the measured energies of the states. Possible reasons for this failure include configuration interaction with other states, spin−orbit interactions with states deriving from other configurations, or both. Configuration interaction with other states will shift the term energies T_Σ, T_Π, and T_Δ, an effect that is taken into account in the model. However, configuration interaction also modifies the electronic wave functions of the $^2\Sigma^+$, $^2\Pi$, and $^2\Delta$ states, possibly changing the magnitude of the spin−orbit interactions, in both the diagonal and off-diagonal terms. This effect is not included in the Hamiltonian of eq 3. In the related molecule, NiH, configurational mixing between the $^2\Sigma^+$ states deriving from the $3d_{Ni}^9\ 3d_{Cu}^{10}\ \sigma^2$ and $3d_{Ni}^{10}\ 3d_{Cu}^{10}\ \sigma^1$ configurations was found to be important, resulting in a lowering of the $^2\Sigma^+$ term energy.[9] In addition, the dilution of $3d_{Ni}^9\ 3d_{Cu}^{10}\sigma^2$ character caused a reduction in the spin−orbit interaction between the $^2\Sigma^+$ and $^2\Pi_{1/2}$ states that could be modeled by multiplying the off-diagonal spin−orbit matrix element given in eq 3 by a constant, C, giving the revised matrix of eq 4:

$$\underline{\underline{\mathbf{H}}} = \begin{array}{c} \begin{matrix} {}^2\Sigma^+_{1/2} & {}^2\Pi_{1/2} & {}^2\Pi_{3/2} & {}^2\Delta_{3/2} & {}^2\Delta_{5/2} \end{matrix} \\ \begin{pmatrix} T_\Sigma & -\sqrt{\frac{3}{2}}\zeta C & 0 & 0 & 0 \\ -\sqrt{\frac{3}{2}}\zeta C & T_\Pi + \frac{\zeta}{2} & 0 & 0 & 0 \\ 0 & 0 & T_\Pi - \frac{\zeta}{2} & -\zeta & 0 \\ 0 & 0 & -\zeta & T_\Delta + \zeta & 0 \\ 0 & 0 & 0 & 0 & T_\Delta - \zeta \end{pmatrix} \end{array} \quad (4)$$

With the parameters T_Σ, T_Π, T_Δ, ζ, and C, it was possible to simultaneously fit all five of the low-lying electronic states of NiH.[9] The final fitted result made physical sense because the fitted value of $\zeta = 594.2 \pm 0.5$ cm^{-1} was quite close to the atomic parameters $\zeta = 602.7$ cm^{-1} and $\zeta = 603.3$ cm^{-1}, which are valid for the Ni^+ ion in its $3d^9$, ^{2}D term and for the Ni atom in its $3d^94s^1$, ^{3}D term, respectively.[9]

Given the importance of configurational mixing between the $3d_{Ni}^9\ 3d_{Cu}^{10}\ \sigma^2$, $^2\Sigma^+$ and $3d_{Ni}^{10}\ 3d_{Cu}^{10}\ \sigma^1$, $^2\Sigma^+$ states in NiH, an attempt was made to include this effect in our model by multiplying the off-diagonal spin−orbit matrix element $\langle {}^2\Sigma^+ | \hat{\mathbf{H}}^{SO} | {}^2\Pi_{1/2} \rangle$ by a constant, C, giving the matrix Hamiltonian of eq 4. This accounted for the configuration interaction described above by diluting the amount of $3d_{Ni}^9\ 3d_{Cu}^{10}\ \sigma^2$, $^2\Sigma^+$ character in the $^2\Sigma^+$ state. We then attempted to fit our four observed electronic states by varying the constants T_Σ, T_Π, T_Δ, and C while holding ζ fixed at 603 cm^{-1}. Regardless of the

TABLE 4: Comparison of Calculational Models to Experimental Assignments for NiCu

state	experimental energy	ab initio[a]	ligand field 1[b]	ligand field 2[c]	fit 3[d]	fit 4[e]
$^1/_2$	not observed	3239	3346.2	3823.1	3057.3	3122.23
$[1.7]^3/_2$	1733.9	1952 (−218)	2098.4 (−365)	2264.2 (−530)	1909.3 (−175)	1799.9 (−66)
$[1.5]^1/_2$[f]	1465.9	1602 (−136)	1775.6 (−310)	2103.8 (−638)	1466.0 (0)	1465.9(0)
$[0.9]^3/_2$[f]	912.4	719 (193)	798.5 (114)	862.4 (50)	697.5 (215)	593.8(64)
$X^2\Delta_{5/2}$	0	0	0	0	38.2 (−38)	−1.618(2)

[a] From ref 34. Experiment minus theory is given in parentheses. [b] As calculated in ref 33 using $\zeta = 603$ cm^{-1} and ligand field parameters of $\langle r^2\rangle_{3d} = 0.3466$ Å^2 and $\langle r^4\rangle_{3d} = 0.3204$ Å^4, which are obtained from Dirac−Fock calculations on the $3d^84s^2$, ^{3}F state of atomic nickel, as reported in ref 43. [c] As calculated using $\zeta = 603$ cm^{-1} and ligand field parameters of $\langle r^2\rangle_{3d} = 0.42697$ Å^2 and $\langle r^4\rangle_{3d} = 0.56244$ Å^4, as are appropriate for the $3d^94s^1$, ^{3}F state of atomic nickel. These are obtained from the numerical Hartree−Fock values,[42] corrected to relativistic values using scaling factors reported in ref 43. [d] This represents the best fit that could be obtained by varying T_Σ, T_Π, and T_Δ, while holding $\zeta = 603$ cm^{-1}, as described in the text. The fitted results of $T_\Sigma = 2557.7$ cm^{-1}, $T_\Pi = 1664.1$ cm^{-1}, and $T_\Delta = 641.2$ cm^{-1} are equivalent to $\langle r^2\rangle_{3d} = 0.2824$ Å^2 and $\langle r^4\rangle_{3d} = 0.4777$ Å.[4] [e] The best fit that could be obtained by varying T_Σ, T_Π, T_Δ, and C, holding $\zeta = 603$ cm^{-1}, and assigning the lowest observed level of the $[0.9]^3/_2$ system as the $v = 1$ level. The fitted values are $T_\Sigma = 2795.7$, $T_\Pi = 1490.9$, $T_\Delta = 601.4$ cm^{-1}, and $C = 0.8922$. See text for details. [f] The value of Ω for this state is not determined experimentally but is based on a comparison to theory.

estimates of these parameters used to initialize the nonlinear least-squares minimization, residuals in the final fit were similar to those listed as Fit 3 in Table 4. A good fit of the data could simply not be obtained with the model of eq 4.

It is disturbing that all of the theoretical treatments of the $3d_{Ni}^9\,3d_{Cu}^{10}\,\sigma^2$ states of NiCu fail to match the measured energy levels. Even Fit 3, which provides the best agreement with experiment, displays residuals in excess of 200 cm^{-1}. Allowing ζ to vary does little to improve the agreement, giving errors as large as 160 cm^{-1} for the best fit, which requires the unphysically small fitted value of $\zeta = 468$ cm^{-1}. To find a better fit than this would require that different values of ζ be used in the various Hamiltonian matrix elements in eq 3, similar to what was done for the $\langle ^2\Sigma^+|\hat{\mathbf{H}}^{SO}|^2\Pi_{1/2}\rangle$ matrix element. However, there is no reason to believe that this should be necessary, given our understanding of the NiCu molecule. With this in mind it is worthwhile to consider the possibility of errors in the experimental measurements.

Every theoretical treatment of the $3d_{Ni}^9\,3d_{Cu}^{10}\,\sigma^2$ states of NiCu presented in Table 4 places the $[1.7]^3/_2$ and $[1.5]^1/_2$ states of NiCu above their observed energies. Likewise, the $[0.9]^3/_2$ state is calculated to lie substantially below its measured energy. Given the weakness of the signal in these dispersed fluorescence experiments, it is possible that some of the vibrational levels of these states were unobserved in our experiments. If some of the lower vibrational levels of the $[1.7]^3/_2$ and $[1.5]^1/_2$ states went undetected, this would place their zero point levels even lower in energy, heightening the discrepancy between the theoretical models and experiment. In the case of the $[0.9]^3/_2$ state, however, if the $v = 0$ level were undetected, the vibrational numbering of the observed levels within this state would have to be increased by 1, which would place the unobserved $v = 0$ level near 658.2 cm^{-1}, greatly improving the agreement with the calculations. Adopting this revised vibrational assignment, working with the Hamiltonian matrix given in eq 3, holding ζ fixed at 603 cm^{-1}, and allowing T_Σ, T_Π, and T_Δ to vary, the fit listed as Fit 4 in Table 4 is obtained. Now the largest residual is only 66 cm^{-1}, an amount that conceivably could result from spin−orbit or configuration interactions with other states. In the hope of finding evidence of the missing vibrational level near 658 cm^{-1}, all of the dispersed fluorescence spectra have been carefully reexamined. Unfortunately, no convincing evidence of its presence was found. A definitive statement on this issue will require more sensitive experiments.

B. Comparison of All Spectroscopically Known NiX Molecules Having a $3d_{Ni}^9$ Core. At present, a large number of monoligated nickel-containing molecules are spectroscopically known in which the nickel atom adopts a $3d_{Ni}^9$ configuration. These include, in order of increasing ligand electronegativity (given on the Pauling scale in parentheses following each compound),[44] AlNi (1.61),[13,14] NiCu (2.00),[10,11] NiH (2.20),[4−6,8,9] NiAu (2.54),[12,13] NiI (2.66),[29,30] NiCN (2.75[45]),[31] NiBr (2.96),[27,28] NiCl (3.16),[21−26] and NiF (3.98).[16−20,46,47] The first six of these molecules exhibit $^2\Delta_{5/2}$ ground states, and the remaining three have $\Omega = ^3/_2$ ground states. The correlation of ground electronic state with the electronegativity of the ligand suggests that a systematic trend in electronic structure exists among these compounds. To examine this in more detail, we have attempted to fit the known energy levels of these molecules to the matrix Hamiltonian of eq 4. The results have been quite successful for NiF, NiCl, and AlNi, where all five low-lying electronic states are known. A very similar approach, with extensions to account for rotation−electronic and vibronic interactions, has been previously applied to NiH by Gray et al.[9] In that investigation, which inspired the present study, a successful analysis of the electronic structure of NiH was also obtained. For NiAu and NiCN, insufficient data are available to provide an unambiguous fit to the matrix Hamiltonian. Spectroscopic studies of NiBr[27,28] and NiI[29,30] have also been reported, but at this time insufficient data are available concerning the $3d_{Ni}^9$ manifold of states to attempt an analysis.

In the case of NiF, recent spectroscopic studies have characterized all five of the low-lying $v = 0$ vibronic levels:[17,19,20] These include states with $\Omega = ^3/_2$ at 0 and 2223 cm^{-1}, $\Omega = ^1/_2$ at 251 and 1574 cm^{-1}, and $\Omega = ^5/_2$ at 829 cm^{-1}. Because all five levels associated with the $3d_{Ni}^9$ configuration have been measured, it is straightforward to fit the values of the ζ, C, T_Σ, T_Π, and T_Δ parameters to this model. The result gives $\zeta = 606.9$, $T_\Sigma = 1038.2$, $T_\Pi = 483.7$, $T_\Delta = 1436.4$ cm^{-1}, and $C = 0.874$. As in the case of NiH, the close agreement between the fitted value of ζ and the accepted values for $3d^9$ Ni^+ and $3d^94s^1$ Ni demonstrates the validity of the model.

All five states of NiCl deriving from the $3d_{Ni}^9$ configuration have also been measured.[21−26] The ground state is again an $\Omega = ^3/_2$ state, whereas the second $\Omega = ^3/_2$ state lies at 1646 cm^{-1}. The $^2\Delta_{5/2}$ level lies at 161 cm^{-1}, and the two $\Omega = ^1/_2$ states lie at 382 and 1768 cm^{-1}. These values can also be fit using the matrix Hamiltonian of eq 4. The result gives $\zeta = 608.2$, $T_\Sigma = 1273.2$, $T_\Pi = 572.7$, $T_\Delta = 769.2$ cm^{-1}, and $C = 0.891$. Again, it is satisfying that the fitted value of ζ falls quite close to the expected value.

In our previous resonant two-photon ionization and dispersed fluorescence studies of AlNi, the ground state was determined to be a $^2\Delta_{5/2}$ state, the low-lying $\Omega = ^3/_2$ states were located at 1078 and 3570 cm^{-1}, and the $\Omega = ^1/_2$ states were found at 2450 and 4210 cm^{-1}.[13,14] In our previous paper on this subject,[13] we erroneously stated that these levels could not be adequately

TABLE 5: Comparison of Electronic Levels and Fitted Parameters for AlNi, NiH, NiCl, and NiF

property	AlNi[a]	NiH[b]	NiCl[c]	NiF[d]
electronic levels and Ω values	4210 ($\Omega = {}^1/_2$)		1768 ($\Omega = {}^1/_2$)	2223 ($\Omega = {}^3/_2$)
	3570 ($\Omega = {}^3/_2$)		1646 ($\Omega = {}^3/_2$)	1574 ($\Omega = {}^1/_2$)
	2450 ($\Omega = {}^1/_2$)		382 ($\Omega = {}^1/_2$)	829 ($^2\Delta_{5/2}$)
	1078 ($\Omega = {}^3/_2$)		161 ($^2\Delta_{5/2}$)	251 ($\Omega = {}^1/_2$)
	0 ($^2\Delta_{5/2}$)		0 ($\Omega = {}^3/_2$)	0 ($\Omega = {}^3/_2$)
		Fitted Values		
ζ (cm^{-1})	622.3	594.2	608.2	606.9
C	0.707	0.855	0.891	0.874
T_Σ (cm^{-1})	2634.3	1826.6	1273.2	1038.2
T_Π (cm^{-1})	3714.6	2212.2	572.7	483.7
T_Δ (cm^{-1})	622.3	0.0	769.2	1436.4
		Derived Quantities		
$\bar{T}$ (cm^{-1})	1861.6	1250.2	791.4	975.7
$T_\Sigma - \bar{T}$ (cm^{-1})	372.7	576.4	481.8	62.5
$T_\Pi - \bar{T}$ (cm^{-1})	1453.0	962.0	−218.7	−492.0
$T_\Delta - \bar{T}$ (cm^{-1})	−1639.3	−1250.2	−22.2	460.7

[a] AlNi electronic levels taken from refs 13 and 14. [b] Fitted parameters for NiH are taken from ref 9. Because the individual rotational levels of several vibronic states were directly fitted, values of T_0 for the various substates are not listed above. [c] NiCl electronic levels are taken from refs 22 and 23. [d] NiF electronic levels are taken from ref 19.

TABLE 6: Calculated Compositions of Spin−Orbit Mixed Electronic States of AlNi, NiCl, and NiF

AlNi level	composition	NiCl level	composition	NiF level	composition
4210 ($\Omega = {}^1/_2$)	10% $^2\Sigma^+$ + 90% $^2\Sigma$	1768 ($\Omega = {}^1/_2$)	64% $^2\Sigma^+$ + 36% $^2\Pi$	2223 ($\Omega = {}^3/_2$)	8% $^2\Pi$ + 92% $^2\Delta$
3570 ($\Omega = {}^3/_2$)	93% $^2\Pi$ + 7% $^2\Delta$	1646 ($\Omega = {}^3/_2$)	16% $^2\Pi$ + 84% $^2\Delta$	1574 ($\Omega = {}^1/_2$)	59% $^2\Sigma^+$ + 41% $^2\Pi$
2450 ($\Omega = {}^1/_2$)	90% $^2\Sigma^+$ + 10% $^2\Pi$	382 ($\Omega = {}^1/_2$)	36% $^2\Sigma^+$ + 64% $^2\Pi$	829 ($^2\Delta_{5/2}$)	100% $^2\Delta$
1078 ($\Omega = {}^3/_2$)	7% $^2\Pi$ + 93% $^2\Delta$	161 ($^2\Delta_{5/2}$)	100% $^2\Delta$	251 ($\Omega = {}^1/_2$)	41% $^2\Sigma^+$ + 59% $^2\Pi$
0 ($^2\Delta_{5/2}$)	100% $^2\Delta$	0 ($\Omega = {}^3/_2$)	84% $^2\Pi$ + 16% $^2\Delta$	0 ($\Omega = {}^3/_2$)	92% $^2\Pi$ + 8% $^2\Delta$

reproduced with a matrix Hamiltonian of the form of eq 4, because the resulting fit required the absurdly large value of $\zeta = 997$ cm^{-1}. Since that time, we have discovered errors in the code used to perform the fit. With the revised software, it turns out that it is indeed possible to find an acceptable fit of these measured energy levels to the matrix Hamiltonian of eq 4. The result gives $\zeta = 622.3$, $T_\Sigma = 2634.3$, $T_\Pi = 3714.6$, $T_\Delta = 622.3$ cm^{-1}, and $C = 0.707$. In this case, the fitted value of ζ is a bit higher than might be expected but may still lie within the range of acceptable values.

Table 5 summarizes the fits of AlNi, NiH, NiCl, and NiF to the matrix Hamiltonian given in eq 4. To place the fitted parameters T_Σ, T_Π, and T_Δ on the same relative scale, so that the trends in these parameters may be appropriately assessed, we have computed the average term energy for the 3d^9 set of states, defined by

$$\bar{T} = \frac{T_\Sigma + 2T_\Pi + 2T_\Delta}{5} \qquad (5)$$

We have then calculated the values of T_Σ, T_Π, and T_Δ relative to this average term energy, as $T_\Sigma - \bar{T}$, $T_\Pi - \bar{T}$, and $T_\Delta - \bar{T}$. These values are listed in Table 5 and plotted in Figure 3 as a function of the Pauling electronegativity of the ligand. The figure displays a clear trend, with the term energy of the $^2\Delta$ state rising and the term energy of the $^2\Pi$ state falling as the electronegativity increases. The term energy of the $^2\Sigma^+$ state remains rather constant as a function of the electronegativity of the ligand. These trends are consistent with the observation that all of the NiX molecules for which X has an electronegativity below 2.85 have $^2\Delta_{5/2}$ ground states, whereas those for which the electronegativity is above 2.85 have $\Omega = {}^3/_2$ ground states that are a spin−orbit induced mixture of the $^2\Pi_{3/2}$ and $^2\Delta_{3/2}$ states. The actual compositions of all of the mixed $\Omega = {}^3/_2$ and $\Omega = {}^1/_2$ states have been derived from the eigenvectors of the matrix Hamiltonian, eq 4 and are listed in Table 6. Clearly, it is

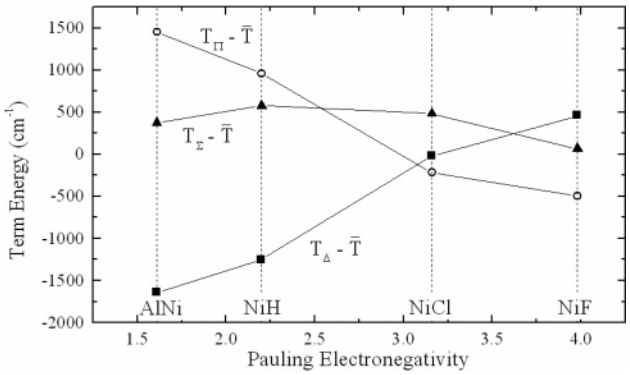

Figure 3. Fitted term energies of the $^2\Sigma^+$, $^2\Pi$, and $^2\Delta$ states of AlNi, NiH, NiCl, and NiF, plotted as a function of the electronegativity of the ligand. A systematic trend is evident.

inappropriate to think of Λ as a good quantum number for some states of these molecules. Spin−orbit induced state mixing is expected to be even more severe in the dense manifold of excited states that are found above 15 000 cm^{-1} in all of these molecules.

It is straightforward to understand why the relative term energies plotted in Figure 3 show the observed trend as a function of the electronegativity of the ligand. One would ordinarily expect the 3d-based orbitals of nickel to fall in the order dσ < dπ < dδ for a positively charged ligand such as Al. This is expected because the electropositive Al atom will stabilize the 3dσ orbital, which is pointed directly toward it, more than the 3dπ orbital, which is in turn stabilized more than the 3dδ orbital. Thus, in AlNi one would expect the hole in the 3d^9 subshell to preferentially lie in the 3dδ orbital, giving a $^2\Delta$ ground term. The $^2\Pi$ term would be expected to lie higher in energy, followed by the $^2\Sigma^+$ term. For a more electronegative ligand, such as F, this energetic ordering is expected to be reversed, with the $^2\Sigma^+$ term lying lowest, followed by the $^2\Pi$ and $^2\Delta$ terms at higher energies. This is precisely the trend that

is seen in Figure 3 for the term energies of the $^2\Pi$ and $^2\Delta$ states. Surprisingly, however, the term energy of the $^2\Sigma^+$ state does not follow the expected trend.

The failure of the $^2\Sigma^+$ term to follow the trend of the $^2\Pi$ and $^2\Delta$ states probably results from the configurational mixing between the $3d^9\sigma^2$ and $3d^{10}\sigma^1$ states of NiH, and the analogues of these states in the cases of AlNi, NiCl, and NiF. Whereas the energies of the $3d\pi$ and $3d\delta$ orbitals are controlled by the electronegativity of the ligand, the $3d\sigma$ orbital is strongly mixed with other orbitals of σ symmetry (in particular, with the 4s orbital of nickel), so that its energy need not follow the trend described above.

V. Conclusion

A dispersed fluorescence investigation of the states of NiCu that derive from the $3d_{Ni}^9\ 3d_{Cu}^{10}\ \sigma^2$ configuration has led to the observation of four out of the five states. Vibrational frequencies and anharmonicities have been derived for the four observed states. The values $\omega_e = 275.93 \pm 1.06\ cm^{-1}$ and $\omega_e x_e = 1.44 \pm 0.11\ cm^{-1}$ have been obtained for the ground $^2\Delta_{5/2}$ state. The pattern of the low-lying electronic states is generally in accord with the predictions of ab initio and ligand field calculations, but errors of a few hundred cm^{-1} in the energies of these states are the norm for all theoretical methods. Attempts to fit the observed states to a ligand field model or to a more general matrix Hamiltonian have not been successful, and it is conjectured that this may be due to experimental difficulties in observing the $v = 0$ level of the lowest excited electronic state.

The low-lying electronic states of AlNi, NiH, NiCl, and NiF have been examined and successfully fitted to a matrix Hamiltonian. The results show that the term energy of the $3d^9\ ^2\Delta$ state increases with increasing ligand electronegativity, whereas the term energy of the $3d^9\ ^2\Pi$ state decreases as the ligand electronegativity is increased. This leads to a change in the ground state as one increases the electronegativity of the ligand, so that AlNi, NiCu, NiH, NiAu, NiI, and NiCN, all of which have a ligand electronegativity below 2.85, have a $^2\Delta_{5/2}$ ground state. In contrast, NiBr, NiCl, and NiF, for which the ligand electronegativity is greater than 2.85, have an $\Omega = {}^3/_2$ ground state that is primarily $^2\Pi$ in character.

Acknowledgment. This material is based upon work supported by the National Science Foundation under Grant No. 0415647.

References and Notes

(1) Scullman, R.; Loefgren, S.; Kadavathu, S. A. *Phys. Scr.* **1982**, *25*, 295.
(2) Gray, J. A.; Rice, S. F.; Field, R. W. *J. Chem. Phys.* **1985**, *82*, 4717.
(3) Gray, J. A.; Field, R. W. *J. Chem. Phys.* **1986**, *84*, 1041.
(4) Adakkai Kadavathu, S.; Loefgren, S.; Scullman, R. *Phys. Scr.* **1987**, *35*, 277.
(5) Li, M.; Field, R. W. *J. Chem. Phys.* **1989**, *90*, 2967.
(6) Gray, J. A.; Li, M.; Field, R. W. *J. Chem. Phys.* **1990**, *92*, 4651.
(7) Hill, E. J.; Field, R. W. *J. Chem. Phys.* **1990**, *93*, 1.
(8) Kadavathu, S. A.; Scullman, R.; Gray, J. A.; Li, M.; Field, R. W. *J. Mol. Spectrosc.* **1990**, *140*, 126.
(9) Gray, J. A.; Li, M.; Nelis, T.; Field, R. W. *J. Chem. Phys.* **1991**, *95*, 7164.
(10) Fu, Z.; Morse, M. D. *J. Chem. Phys.* **1989**, *90*, 3417.
(11) Spain, E. M.; Morse, M. D. *J. Chem. Phys.* **1992**, *97*, 4633.
(12) Spain, E. M.; Morse, M. D. *J. Chem. Phys.* **1992**, *97*, 4605.
(13) Fabbi, J. C.; Karlsson, L.; Langenberg, J. D.; Costello, Q. D.; Morse, M. D. *J. Chem. Phys.* **2003**, *118*, 9247.
(14) Behm, J. M.; Arrington, C. A.; Morse, M. D. *J. Chem. Phys.* **1993**, *99*, 6409.
(15) Focsa, C.; Dufour, C.; Pinchemel, B. *J. Mol. Spectrosc.* **1997**, *182*, 65.
(16) Chen, Y.; Jin, J.; Hu, C.; Yang, X.; Ma, X.; Chen, C. *J. Mol. Spectrosc.* **2000**, *203*, 37.
(17) Jin, J.; Ran, Q.; Yang, X.; Chen, Y.; Chen, C. *J. Phys. Chem. A* **2001**, *105*, 11177.
(18) Jin, J.; Chen, Y.; Yang, X.; Ran, Q.; Chen, C. *J. Mol. Spectrosc.* **2001**, *208*, 18.
(19) Krouti, Y.; Hirao, T.; Dufour, C.; Boulezhar, A.; Pinchemel, B.; Bernath, P. F. *J. Mol. Spectrosc.* **2002**, *214*, 152.
(20) Pinchemel, B.; Hirao, T.; Bernath, P. F. *J. Mol. Spectrosc.* **2002**, *215*, 262.
(21) Hirao, T.; Dufour, C.; Pinchemel, B.; Bernath, P. F. *J. Mol. Spectrosc.* **2000**, *202*, 53.
(22) Poclet, A.; Krouti, Y.; Hirao, T.; Pinchemel, B.; Bernath, P. F. *J. Mol. Spectrosc.* **2000**, *204*, 125.
(23) Krouti, Y.; Poclet, A.; Hirao, T.; Pinchemel, B.; Bernath, P. F. *J. Mol. Spectrosc.* **2001**, *210*, 41.
(24) O'Brien, J. J.; Miller, J. S.; O'Brien, L. C. *J. Mol. Spectrosc.* **2002**, *211*, 248.
(25) O'Brien, L. C.; Homann, K. M.; Kellerman, T. L.; O'Brien, J. J. *J. Mol. Spectrosc.* **2002**, *211*, 93.
(26) Rice, C. A.; O'Brien, L. C. *J. Mol. Spectrosc.* **2003**, *221*, 131.
(27) Leung, J. W. H.; Wang, X.; Cheung, A. S. C. *J. Chem. Phys.* **2002**, *117*, 3694.
(28) Yamazaki, E.; Okabayashi, T.; Tanimoto, M. *J. Chem. Phys.* **2004**, *121*, 162.
(29) Tam, W. S.; Leung, J. W. H.; Hu, S.-M.; Cheung, A. S. C. *J. Chem. Phys.* **2003**, *119*, 12245.
(30) Tam, W. S.; Ye, J.; Cheung, A. S. C. *J. Chem. Phys.* **2004**, *121*, 9430.
(31) Kingston, C. T.; Merer, A. J.; Varberg, T. D. *J. Mol. Spectrosc.* **2002**, *215*, 106.
(32) Sheridan, P. M.; Ziurys, L. M. *J. Chem. Phys.* **2003**, *118*, 6370.
(33) Spain, E. M.; Morse, M. D. *J. Chem. Phys.* **1992**, *97*, 4641.
(34) Shim, I. *Theor. Chim. Acta* **1980**, *54*, 113.
(35) Hopkins, J. B.; Langridge-Smith, P. R. R.; Morse, M. D.; Smalley, R. E. *J. Chem. Phys.* **1983**, *78*, 1627.
(36) Fabbi, J. C. P. Spectroscopy of Transition Metal Dimers and Trimers. Ph.D., University of Utah, 1995.
(37) O'Brien, S. C.; Liu, Y.; Zhang, Q.; Heath, J. R.; Tittel, F. K.; Curl, R. F.; Smalley, R. E. *J. Chem. Phys.* **1986**, *84*, 4074.
(38) Morse, M. D.; Hansen, G. P.; Langridge-Smith, P. R. R.; Zheng, L.-S.; Geusic, M. E.; Michalopoulos, D. L.; Smalley, R. E. *J. Chem. Phys.* **1984**, *80*, 5400.
(39) Pinegar, J. C.; Langenberg, J. D.; Arrington, C. A.; Spain, E. M.; Morse, M. D. *J. Chem. Phys.* **1995**, *102*, 666.
(40) Phelps, F. M. *Massachusetts Institute of Technology wavelength tables*; MIT Press: Cambridge, MA, 1969; Vol. 2.
(41) Bevington, P. R. *Data Reduction and Error Analysis for the Physical Sciences*; McGraw-Hill: New York, 1969.
(42) Fischer, C. F. *The Hartree−Fock Method for Atoms*; John Wiley & Sons: New York, 1977.
(43) Desclaux, J. P. *At. Data Nucl. Data Tables* **1973**, *12*, 311.
(44) Huheey, J. E. *Inorganic Chemistry*; Harper & Row: New York, 1983.
(45) Constantinides, E. *Proc. Chem. Soc.* **1964**, 290.
(46) Bouddou, A.; Dufour, C.; Pinchemel, B. *J. Mol. Spectrosc.* **1994**, *168*, 477.
(47) Dufour, C.; Hikmet, I.; Pinchemel, B. *J. Mol. Spectrosc.* **1994**, *165*, 398.